PCCP

Accepted Manuscript

ROYAL SOCIETY OF CHEMISTRY

www.rsc.org/pccp

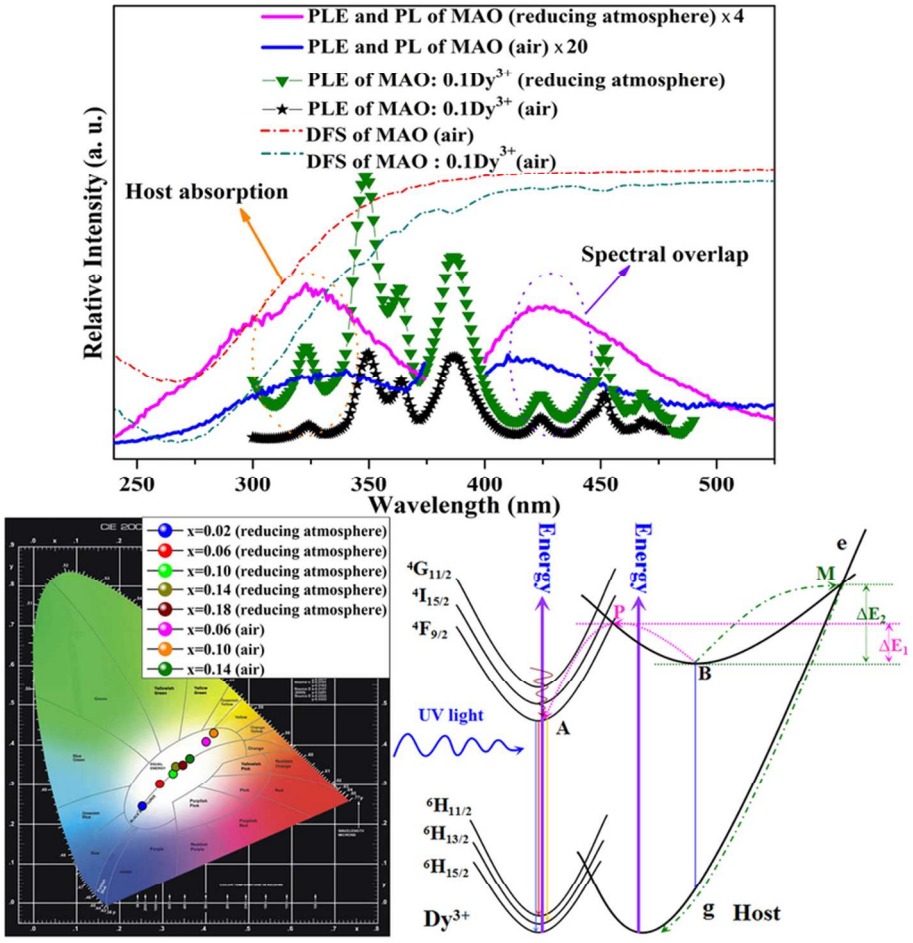

Figure for graphical abstract
40x40mm (600 x 600 DPI)

Warm white light generation from a single phase Dy^{3+} doped $Mg_2Al_4Si_5O_{18}$ phosphor for white UV-LEDs

Zhipeng Ci[*a], Qisheng Sun[a], Shengchun Qin[a], Mengxing Sun[a], Xiaojing Jiang[a], Xudong Zhang[a], Yuhua Wang[*a]

A single phase white-emitting $Mg_2Al_4Si_5O_{18}$: Dy^{3+} phosphor was synthesized and the photoluminescence, energy-transfer mechanism and thermal properties are carefully investigated.

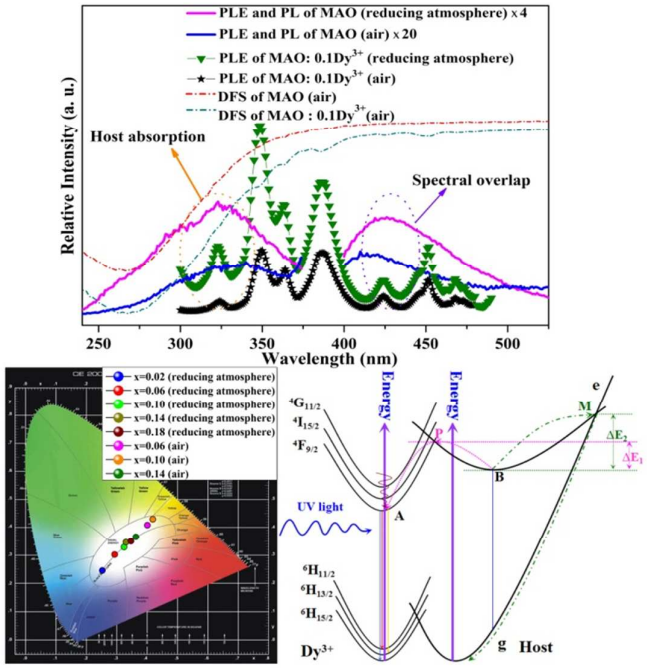

Cite this: DOI: 10.1039/c0xx00000x

www.rsc.org/xxxxxx

ARTICLE TYPE

Warm white light generation from a single phase Dy^{3+} doped $Mg_2Al_4Si_5O_{18}$ phosphor for white UV-LEDs

Zhipeng Ci[*a], Qisheng Sun[a], Shengchun Qin[a], Mengxing Sun[a], Xiaojing Jiang[a], Xudong Zhang[a], Yuhua Wang[*a]

Received (in XXX, XXX) Xth XXXXXXXXX 20XX, Accepted Xth XXXXXXXXX 20XX
DOI: 10.1039/b000000x

Abstract

A series of the samples $Mg_{2-x}Al_4Si_5O_{18}$: xDy^{3+} ($0 \le x \le 0.18$) were firstly synthesized by the solid state method in the reducing atmosphere and air, respectively. XRD, diffuse reflection spectra, excitation spectra, emission spectra, decay times and thermal quenching are tested to investigate the structure, photoluminescence, energy transfer and thermal properties. The results show that the $Mg_2Al_4Si_5O_{18}$: Dy^{3+} can efficiently absorb the UV light, and emit the violet-blue light ranged from 400 to 500 nm from the oxygen vacancies in the host , the blue light (~480 nm) and the yellow light (~576 nm) from the f-f transitions of Dy^{3+}. The emission intensities of samples obtained in the reducing atmosphere are far superior to that of the samples obtained in the air due to the efficient energy transition from the oxygen vacancies in host to Dy^{3+}. The analysis of thermal quenching manifests that the phosphor $Mg_2Al_4Si_5O_{18}$: Dy^{3+} has excellent thermal properties. The emission intensities of typical samples synthesized in the reducing atmosphere and air at 250 ℃ are 70% and 81% of its initial intensities at 20 ℃, respectively. In addition, the emission colors of all samples locate at the white light region, and the optimal chromaticity coordinates and Correlated Color Temperature are (x=0.34, y=0.33) and 5129 K. Thereby, the white $Mg_2Al_4Si_5O_{18}$: Dy^{3+} phosphor can serve as a promising candidate for white-light UV-LEDs.

1. Introduction

In recent years, with the development of photoelectric technology and material science, white-light-emitting diodes (WLEDs) are regarded as a new generation of lighting source after incandescent lamp and energy saving lamp because they are environmentally friendly and energy saving [1, 2]. Among the ways of achieving white light, phosphor-converted (pc) white LEDs has attracted a great attention due to the high efficiency and low cost. There are two methods to obtain white light emission. One is the combination of blue LED with yellow phosphor (YAG: Ce^{3+}), however, this approach makes a poor color rendering index (Ra = 70-80) and high Correlated Color Temperature (CCT ≈ 7750 K) because of the lack of sufficient red component [3, 4]. The other is the combination of ultra-violet (UV) LED with red-green-blue (RGB) phosphors, which also have some disadvantages such as low luminescent efficiency owing to the strong reabsorption of the blue light by the red and green phosphors [5, 6]. Concerning those problems, developing a single-phase white-light emitting phosphor is one of the effective solutions, and has attracted much attention in white LEDs application [7].

At present, among the large number of photoluminescence materials, rare-earth doped silicate phosphors are well known for their high efficiency and good chemical stability, [8-16] and have been applied in the LED, PDP and FED filed such as $ZnSiO_4$: Mn^{2+}, Sr_2SiO_4: Eu^{2+} and $M_3MgSi_2O_8$: Eu^{2+}, Mn^{2+} (M=Ca, Sr, Ba), and so on [17-19]. As an extremely versatile material, cordierite silicate $Mg_2Al_4Si_5O_{18}$ (MAO) has been widely used as a high quality refractory materials, integrated circuit board, catalyst carrier, ceramic foam and aviation materials etc., due to its good thermal shock resistance, dielectric properties, fire resistance and mechanical properties [20, 21]. In 2003, Thim [22] studied the luminescence properties of Eu^{3+} doped MAO. However the photoluminescence properties of other rare earth ions doped MAO has not been reported. As an important dopant, Dy^{3+} is widely used in the luminescent materials due to various transitions between different energy levels in the UV-Visible and Near Infrared (NIR) region. Many researches show Dy^{3+} can not only be applied in the WLED and mercury-free luminescence lamps because of the white emission from two dominant bands of blue (470 ~ 500 nm) and yellow (570 ~ 600 nm) [23, 24], but also be frequently used in the light conversion materials by combining with other rare earth ions like Er^{3+} and Yb^{3+}. In addition, Dy^{3+} also usually plays an important role in many long-lasting phosphors, such as $Sr_2Al_2O_4$: Eu^{2+}, Dy^{3+} [25], $Sr_2MgSi_2O_7$: Dy^{3+} [26], and Mg_2SiO_4: Dy^{3+}, Mn^{2+} [27]. Therefore, in order to develop a single phase white emitting phosphor and the basic research, in this paper, we have synthesized a series of the samples $Mg_{2-x}Al_4Si_5O_{18}$: xDy^{3+} ($0 \le x \le 0.18$) by the solid state method in the reducing atmosphere and air, and carefully investigated the photoluminescence, mechanism of energy transfer and thermal properties.

2. Experimental

2.1 Materials and synthesis

Stoichiometric amounts of $(MgCO_3)_4{\cdot}Mg(OH)_2{\cdot}5H_2O$ (AR), Al_2O_3 (AR), SiO_2 (AR), Dy_2O_3 (AR) and NH_4Cl (AR) (3wt%, as a flux) as the raw materials were thoroughly mixed in an agate

mortar by using ethanol. Firstly, the mixture was heated up to 600 ℃ for 6 h, then the mixture was reground and further fired at 1400 ℃ for 10 h in an alumina crucible under the air and N_2-H_2 (8%) atmosphere in horizontal tube furnace, and then slowly cooled to the room temperature. Finally, the two samples synthesized in the air and reducing atmosphere were obtained.

2.2 Measurements and characterization

The crystal structures of the synthesized samples were identified by using a Rigaku D/Max-2400 X-ray diffractometer with Ni filtered CuKa radiation (XRD). Diffuse reflection spectra were obtained by a UV/visible spectrophotometer (Perkin-Elmer Lambda 950) using $BaSO_4$ as a reference in the range of 240-700 nm. The photoluminescence (PL), photoluminescence excitation (PLE) spectra of the samples were measured using an FLS-920T fluorescence spectrophotometer equipped with a 450 W Xe light source, Xe Flash Lamp and ns pulsed hydrogen lamp. The quantum efficiency was measured by a Fluorlog-3 spectrofluorometer equipped with a 450 W xenon lamp (Horiba Jobin Yvon). All of the measurements were performed at room temperature. Thermal quenching was tested using a heating apparatus (TAP-02) in combination with PL equipment.

3. Results and Discussion

3.1 Crystal Structure of MAO

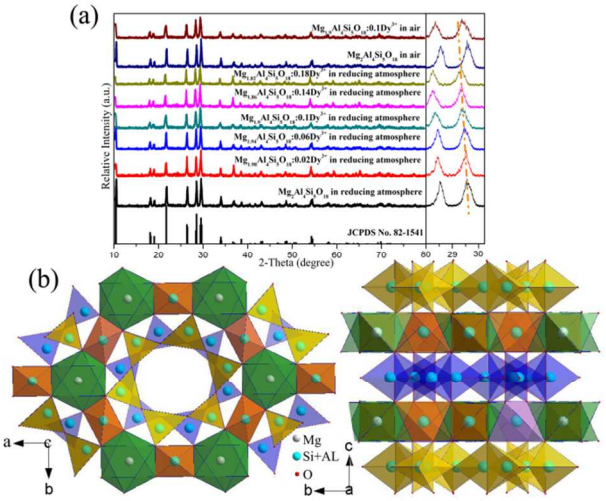

Figure 1 (a) The XRD patterns of samples MAO: xDy^{3+} ($0 \le x \le 0.18$) synthesized in the reducing atmosphere and air; (b) The structure diagram of MAO.

Figure 1(a) shows the XRD patterns of samples MAO: xDy^{3+} ($0 \le x \le 0.18$) synthesized in the reducing atmosphere and air. All the observed diffraction peaks are well indexed to the phases of $Mg_2Al_4Si_5O_{18}$ (JCPDS No. 82-1541) and no second phase is observed, indicating that the doping ions do not cause significant changes in the host. Figure 1(b) presents the structure diagram of MAO. Cordierite MAO, with an ideal composition $Mg_2Al_4Si_5O_{18}$, is a Mg aluminisilicate. It belongs to orthorhombic structure (space group Cccm) with four molecules in the unit cell. In the structure, there is only one Mg^{2+} site coordinated by 6 O^{2-}. Si^{4+} and Al^{3+} are both surrounded by 4 O^{2-} and form a tetrahedra. Similar to those of beryl, the Si/Al-tetrahedras form Si_6O_{18}-type 6-membered-rings with one Al substituted for one Si in the ring. The Si atoms in the rings are bonded to two oxygen atoms in the ring and to two oxygen atoms in layers above and below. There is no direct bonding between rings, but they are linked by Mg in octahedra and by Al in tetrahedra above and below [28]. When doping ions are introduced into the MAO host, in principle, it could be incorporated on any one of the three cation sites [29, 30], i.e. Mg^{2+} (ionic radius of 0.72 Å), Al^{3+} (0.39 Å) and Si^{4+} (0.26 Å) (ionic radii from ref. 31 and Table1). The effective ionic radius of Dy^{3+} is 0.91 Å (for sixfold coordinated Dy^{3+}; data on fourfold coordination are presently not available) [31]. Comparison of ionic radii mismatch, however, points to Mg^{2+}-sites as the most probable host for Dy^{3+}. In addition, according to the reports of Sai [32] and Tang [33], the Mg^{2+} (0.72Å) in MAO can be replaced by the bigger ions Ca^{2+} (1.00 Å) [31], Sr^{2+} (1.18 Å) [31] and Ba^{2+} (1.35Å) [31] to form the solid solution. Therefore, it is possible that the Dy^{3+} is introduced into the MAO host, and in Figure 1(a), it is obviously observed that the XRD peaks lightly shift to smaller angle due to the bigger radius of Dy^{3+} than Mg^{2+}.

Table 1 Relative difference in ionic radii (Dr(%) = 100×[R_m(CN)-R_d(CN)]/R_m(CN)) between matrix cations and dopant Dy^{3+}.

Ions	Radius/Å	CN	Dr(%)
Dy^{3+}	0.91	6	0
Mg^{2+}	0.72	6	-26.39
Al^{3+}	0.39	4	-133.33
Si^{4+}	0.26	4	-250

3.2 Photoluminescence properties analysis

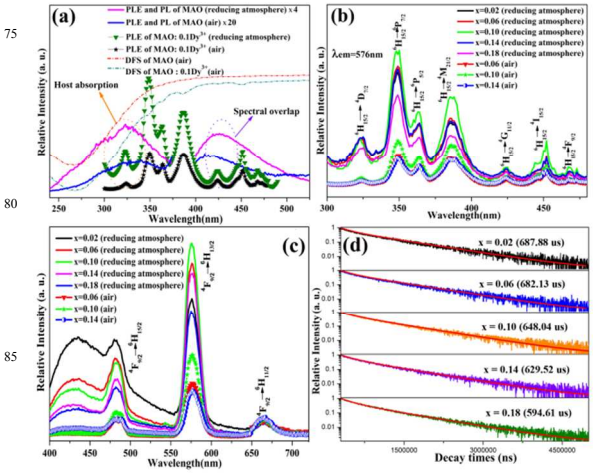

Figure 2 (a) The PLE (λ_{em} = 425 nm) and PL (λ_{ex} = 325 nm) spectra of MAO, the PLE (λ_{em} = 576 nm) spectra of MAO: 0.1Dy^{3+} synthesized in the reducing atmosphere and air and the DFS of MAO and MAO: 0.1Dy^{3+} obtained in the air; (b) and (c) The PLE (λ_{em} = 576 nm) and PL (λ_{ex} = 350 nm) spectra of MAO: xDy^{3+} synthesized in the reducing atmosphere and air; (d) The decay curves of MAO: xDy^{3+} with different Dy^{3+} contents (λ_{ex} = 386 nm, λ_{em} = 576 nm) synthesized in the reducing atmosphere.

In Figure 2(a), the dot lines present the diffuse reflection spectra (DFS) of MAO and MAO: 0.1Dy^{3+} synthesized in the air. Both samples present a remarkable drop in the ultraviolet (UV) range from 200 to 380 nm due to the absorption of the host. Compared with the pure MAO, some new sharp drops at 347, 364, 386, 425 and 453 nm in the DFS of MAO: 0.1Dy^{3+} are observed and can

be ascribed to the characteristic transitions $^6H_{15/2} \rightarrow {}^6P_{7/2}$, $^6P_{5/2}$, $^4M_{21/2}$, $^4G_{11/2}$ and $^4I_{15/2}$ of Dy^{3+}. [34] Photoluminescence spectra of MAO show the sample MAO synthesized in the air can be excited by the UV light from 250 to 380 nm and emit the blue light from 400 to 500 nm. In order to find the reasons of self-illumination, another sample MAO is synthesized in the reducing atmosphere. It is obviously observed that the shapes of PLE and PL spectra of both samples are very similar, but the emission intensity of MAO synthesized in the reducing atmosphere is far above that of sample synthesized in the air. It implies that the blue broad emission band could mainly result from the oxygen vacancies in MAO host. The detailed reasons are shown in the Supporting Information, Figure S1, S2. The PLE spectra of MAO: $0.1Dy^{3+}$ synthesized in the reducing atmosphere and air are also presented in Figure 2(a). There is an obvious spectral overlap between the PL of MAO and PLE of MAO: $0.1Dy^{3+}$, which suggests that an energy transfer between Dy^{3+} and the oxygen vacancies in MAO host could occur. Figure 2(b) and (c) show the PLE (λ_{em} = 576 nm) and PL (λ_{ex} = 350 nm) spectra of MAO: xDy^{3+} synthesized in the reducing atmosphere and air. The sharp excitation peaks from 350 to 470 nm can be attributed to the intra-4f forbidden transitions from the ground level $^6H_{15/2}$ to higher energy levels of Dy^{3+} [35], which is consistent with the DRS of MAO: Dy^{3+} in Figure 2(a). An ideal phosphor for UV-LEDs should have strong absorption from about 350 to 410 nm (emission wavelengths of UV-LED chips) [36, 37]. Obviously, excitation spectra of MAO: xDy^{3+} exhibit strong absorption from around 350 to 410 nm, indicating it can be a candidate as a yellow or white phosphor for UV-LEDs. The emission spectra mainly consist of a broad band from 400 to 500 nm and three characteristic emission peaks located at 482, 576 and 665 nm, respectively, which is attributed to the emission of oxygen vacancies in MAO host and the $^4F_{9/2}$-$^6H_{15/2}$, $^4F_{9/2}$-$^6H_{13/2}$ and $^4F_{9/2}$-$^6H_{11/2}$ transitions of Dy^{3+}, respectively. With the increase of Dy^{3+}, the emission intensities of Dy^{3+} gradually increase, but those of oxygen vacancies in MAO host gradually decrease, which also supports that there is an energy transfer between Dy^{3+} and the oxygen vacancies in MAO host. For the samples synthesized in the reducing atmosphere and air, the optimal Dy^{3+} amount is both at x = 0.1. This critical concentration (5%) is referred to as "quenching concentration". In general, concentration-quenching effect is due to the non-radiative energy transfer process between the neighboring Dy^{3+} when the Dy^{3+} concentration reaches a critical value. Therefore quenching concentration can be more accurately obtained by the changes of decay times of Dy^{3+}. The Figure 2(d) shows the decay times depended on Dy^{3+} contents excited at 386 nm and monitored at 576 nm. The decay times (τ) are calculated to be 687.88, 682.13, 648.04, 629.52 and 594.61 μs with the Dy^{3+} contents from 1% to 9%, respectively. It obviously observed that the decay times gradually decrease and when the Dy^{3+} content x reaches 5%, the decay time sharply declines, which indicates that the energy transfer between Dy^{3+} and Dy^{3+} might occur. Thereby, the quenching concentration is further confirmed at 5% by the changes of decay times. The quantum efficiency of the optimal sample MAO: $0.1Dy^{3+}$ synthesized in the reducing atmosphere is 18.1%. As an important parameter to evaluate the photoluminescence properties, the critical distance R_c of energy transfer between Dy^{3+} and Dy^{3+} could be calculated by the critical concentration of the activator ion [38, 39]:

$$R_c \approx 2\left(\frac{3V}{4\pi x_c N}\right)^{1/3}$$

Where V is the volume of the unit cell, x_c is the critical concentration of the activator ion, and N is the number of cations of per unit cell. For the MAO host, N = 8, x_c = 0.05, and V= 1550.48 Å^3, and the R_c value was calculated to about 19.49 Å.

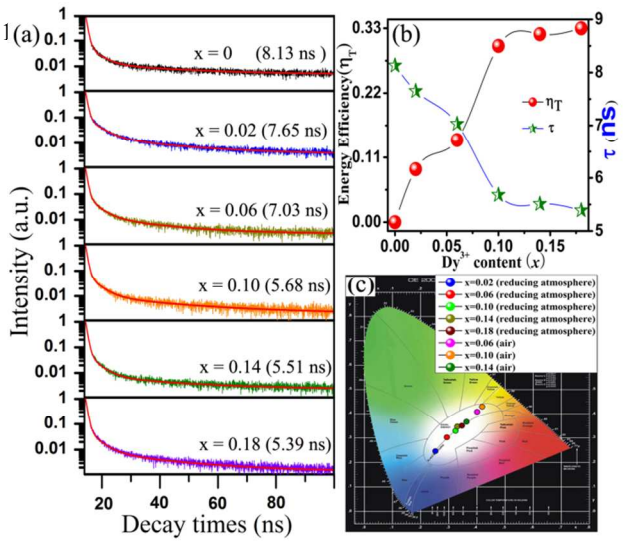

Figure 3 (a) The decay curves of MAO: xDy^{3+} with different Dy^{3+} contents (λ_{ex} = 325 nm, λ_{em} = 425 nm); (b) The relationship between decay times and energy transfer efficiency with the increase of Dy^{3+} contents; (c) The CIE chromaticity coordinates of the samples MAO: xDy^{3+} synthesized in the reducing atmosphere and air.

To further understand the process of energy transfer, the decay times of MAO: xDy^{3+} with different Dy^{3+} contents excited at 325 nm and monitored at 425 nm are measured and depicted in Figure 3(a). The corresponding luminescent decay curves can be fitted by a multi-exponential mode. The average decay times are calculated and listed in Figure 3(a). The PL decay times of the MAO decreases from 8.13 to 5.39 ns when the Dy^{3+} concentration is increased to 9%. The energy transfer efficiency η is defined as the ratio between the number of depopulation events which result in energy transfer from donor to acceptor and the total population of the excited states in the donor. It can be calculated from the ratio of the decay times of the excited state(s) of the donor in the presence of the acceptor as compared to a specimen which contains only the donor species. [40, 41] Therefore, the energy transfer efficiency $\eta_{MAO\text{-}Dy}$ can be obtained by:

$$\eta = 1 - \frac{\tau_s}{\tau_{s0}}$$

Where τ_{S0} is the decay time of the host MAO in the absence of the Dy^{3+} and τ_S is the decay time of the host MAO in the presence of the Dy^{3+}. The decay times are used for calculation, and the results are presented in Figure 3(b). With the increase of Dy^{3+}, the energy transfer efficiency $\eta_{MAO\text{-}Dy}$ increases from 9% to 33%. Figure 3(c) shows the Commission International de L' Eclairage

(CIE) chromaticity coordinates of the samples calculated based on their corresponding PL spectra. The emission colors of all the samples locate at the white light region with the optimal chromaticity coordinates and CCT are (x=0.34, y=0.33) and 5129 K, which is very close to the standard white (x=0.33, y=0.33). The detailed chromaticity coordinates and CCT are listed in Table 2.

Table 2 The detailed data of emission colors, CIE and CCT of MAO: xDy^{3+} synthesized in the reducing atmosphere and air, and blue chips +YAG

Samples compositions	color	CIE		CCT
		x	y	(K)
MAO:0.02Dy^{3+}(reducing)	blue white	0.26	0.25	-
MAO:0.06Dy^{3+}(reducing)	white	0.31	0.30	6936
MAO:0.10Dy^{3+}(reducing)	white	0.34	0.33	5129
MAO:0.14Dy^{3+}(reducing)	white	0.34	0.35	5192
MAO:0.18Dy^{3+}(reducing)	white	0.35	0.35	4798
MAO:0.06Dy^{3+}(air)	warm white	0.41	0.41	3510
MAO:0.10Dy^{3+}(air)	warm white	0.42	0.43	3456
MAO:0.14Dy^{3+}(air)	warm white	0.36	0.36	4493
blue chips +YAG	white	0.29	0.30	5610

3.3 Thermal properties analysis

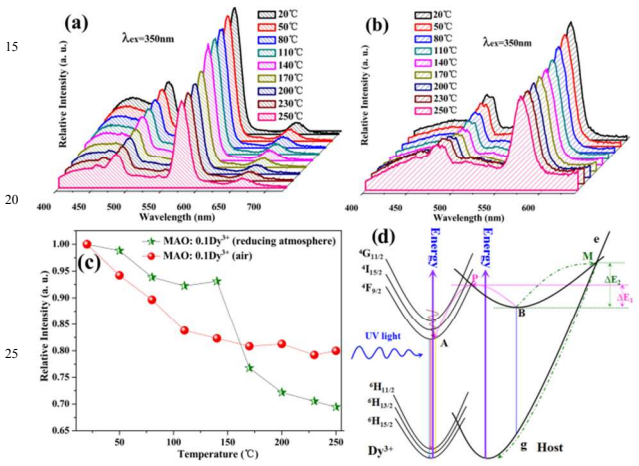

Figure 4 The PL spectra of MAO: 0.1Dy^{3+} synthesized in the reducing atmosphere (a) and air (b) under various temperatures; (c) The dependence of normalized PL intensities on temperature for phosphors; (d) The configurational coordinate diagram of the ground and excited states of Dy^{3+}and the oxygen vacancies in MAO host.

In general, in the process of the phosphors application, the emission intensities of phosphors are reduced by thermal phonon-assisted relaxation, through the crossing point between the excited and the ground states [42-45]. Thereby, the thermal quenching characteristics are greatly of significance for phosphors. The temperature dependent luminescence properties for MAO: 0.1Dy^{3+} synthesized in the reducing atmosphere and air are traced in the temperature ranged from 20 to 250 ℃, and the results are shown in Figure 4(a) and (b). With increasing temperature, the emission intensities of all samples gradually decline. The emission intensities of MAO: 0.1Dy^{3+} synthesized in the reducing atmosphere and air are 70% and 81% of their initial intensities at 20 ℃, which indicates that the phosphor MAO: 0.1Dy^{3+} has excellent thermal stabilities. Figure 4(c) presents that the normalized emission intensity of MAO: 0.1Dy^{3+} synthesized in the reducing atmosphere are obvious above those of the sample synthesized in the air below 150 ℃, and then rapidly decline when the temperature exceeds 150 ℃. The phenomenon could be explained by the configurational coordinate diagram in Figure 4(d). The curves of ^6H_j (j = 11/2, 13/2 and 15/2) and $^4G_{11/2}$, $^4I_{15/2}$ and $^4F_{9/2}$ are the ground and excited states of Dy^{3+}, respectively. The curves of g and e are the ground and excited states of the oxygen vacancies in MAO host, respectively. The points A and B are the lowest position of the curves $^4F_{9/2}$ and e, respectively. The point M is the crossing point of curves e and g, the point P is the crossing point of curves e and the excited states of Dy^{3+}. In order to simplify the discussion, only one crossing point of e and the excited states of Dy^{3+} (P) is marked. At the room temperature, the electrons of ^6H_j and g are firstly excited to the excited states under the excitation of 350 nm. For the excited states of Dy^{3+}, most of electrons return to the ground states by the radiative transition. But for the excited state e, besides the radiative transition, some percentage of the electrons of e would very likely overcome the energy barrier ΔE_1 and transfer the energy to ^6H_j due to the electron-phonon coupling, and thereby the emission intensity of Dy^{3+} is enhanced. With the increase of temperature, more electrons of the excited state e could overcome the energy barriers ΔE_1 due to the stronger electron-phonon coupling, and transfer to the excited states of Dy^{3+} from the crossing points P, which consequently slow down the decline of emission intensity of Dy^{3+}. However, with the further increase of temperature, the electrons of the excited states e would also probably overcome the energy barrier ΔE_2 under the stronger phonon vibration, and direct-tunnel to the ground state g, which results in the rapid decrease of the energy transfer efficiency between the oxygen vacancies in MAO host and Dy^{3+}, and further the emission intensity of Dy^{3+} sharply declines when the temperature is above about 150 ℃. Meanwhile, from Figure 2(c), the emission intensity of Dy^{3+} in MAO: Dy^{3+} synthesized in the reducing atmosphere is far above that in the sample synthesized in the air. It indicates that the emission intensity of Dy^{3+} is seriously influenced by the oxygen vacancies in MAO host. Therefore, with rapid decrease of the energy transfer efficiency between the oxygen vacancies and Dy^{3+}, the thermal property of MAO: Dy^{3+} synthesized in the reducing atmosphere becomes worse than that of the sample synthesized in the air in the normalized intensities of temperature-dependent PL spectra (see in Figure 4(c)).

Conclusions

In conclusion, a series of novel single phase white-emitting phosphors MAO: xDy^{3+} ($0 \le x \le 0.18$) have been synthesized by the solid state method in the reducing atmosphere and air. The luminescence properties, thermal stability as well as the mechanism of energy transfer from the oxygen vacancies in

MAO host to Dy^{3+} are carefully investigated for the first time. Upon 350 nm excitation, the phosphor can exhibit a blue broad band centered at 425 nm due to the emission of the oxygen vacancies and two sharp peaks at 480 and 576 nm ascribed to the f-f transitions of Dy^{3+}, respectively. Because of the energy transfer from the oxygen vacancies to Dy^{3+}, the emission intensities of MAO: Dy^{3+} obtained in the reducing atmosphere are far stronger than that of the samples obtain in the air. More importantly, the wavelength-tunable white light can be realized with the optimal CIE chromaticity coordinates (0.34, 0.33) and CCT 5129 K. The temperature-dependent PL spectra manifest that MAO: 0.1 Dy^{3+} has excellent thermal properties. The emission intensities of MAO: $0.1Dy^{3+}$ synthesized in the reducing atmosphere and air at 250 ℃ are 70% and 81% of its initial intensities at 20 ℃, respectively. In addition, the emission intensity of MAO: $0.1Dy^{3+}$ obtained in the reducing atmosphere is superior to that of the sample obtained in the air when the temperature is below 150 ℃, but the opposite case is presented when the temperature exceeds 150 ℃. By the configurational coordinate diagram, the phenomenon could be reasonably explained. All the results indicate that MAO: Dy^{3+} could serve as a potential single phase white-emitting phosphor for white-light UVLED devices.

Acknowledgment

This work has been supported by the Young Scientists Fund of the National Natural Science Foundation of China (Grant No. 51302121) and the Nature Science Foundation of Gansu Province (Grant Number: 1107RJZA206).

Notes and references

[a] *Department of Materials Science, School of Physical Science and Technology, Lanzhou University, Lanzhou 730000, China, Fax.: +86-931-8913554 (Office), Tel.: +86-931-8912772 (Office), E-mail: cizhp@lzu.edu.cn.*

†Electronic Supplementary Information (ESI) available: Figure S1 shows the PLE and PL spectra of un-doped MAO samples and PL spectra of Dy^{3+} doped MAO samples in the air and reducing atmosphere. Figure S2 presents the Dy 4d XPS spectrum of the MAO: $0.18Dy^{3+}$ sample synthesized in the reducing atmosphere. See DOI: 10.1039/b000000x/

1 P. F. Smet, K. Korthout, J. E. Haecke, D. Poelman, *Mater. Sci.Eng. B* 2007, **146**, 264.
2 M. M. Haque, H. I. Lee, D. K. Kim, *J. Alloys Compd.*, 2009, **481**, 792.
3 K. P. Joung, H. K. Chang, H. P. Seung, D. P. Hee, Y. C. Se, *Appl. Phys. Lett.*, 2004, **84**, 1647.
4 Y. Hu, W. Zhuang, H. Ye, D. Wang, S. Zhang, X. Huang, *J. A lloy. Compd.*, 2005, **390**, 226
5 M. A. Lim,J. K. Park, C. H. Kim, H. D. Park, M. W. Han, *J. Mater. Sci. Lett.*, 2003, 22, 1351.
6 J. Y. Kuang, Y. L. Liu, *Chem.Lett.*, 2005, **34**, 59.
7 J. S. Kim, P. E. Jeon, J. C. Choi, H. L. Park, S. I. Mno, G. C. KIM, *Appl. Phys. Lett.*, 2004, **84**, 2931.
8 X. Yang, S. T. Tan, X. Yu, H. V. Demir, X. W. Sun, *ACS Appl.Mater. Inter.*, 2011, **3**, 4431.
9 B. Wang, L. Sun, H. Ju, *Solid State Commun.*, 2010, **150**, 146.
10 W. J. Yang, L. Luo, T. M. Chen, N. S. Wang, *Chem. Mater.*, 2005, **17**, 3883.
11 D. S. Jo, Y. Y. Luo, K. Senthil, K. Toda, B. S. Kim, T. Masaki, D. H. Yoon, *Opt. Mater.*, 2011, **34**, 696.
12 X. Yu, X. Xu, P. Yang, Z. Yang, Z. Song, D. Zhou, Z. Yin, Q. Jiao, J. Qiu, *Mater. Res. Bull.*, 2012, **47**, 117.
13 M. D. Que, Z. P. Ci, Y. H. Wang, G. Zhu, S. Y. Xin, Y. R. Shi, Q. Wang, *CrystEngComm*, 2013,**15**, 6389.
14 W. Lu, Z. Hao, X. Zhang, Y. Luo, X. Wang, J. Zhang, *Inorg.Chem.*, 2011, **50**, 7846.
15 J. Y. Han, W. B. Im, D. Kim, S. H. Cheong, G. Lee, D. Y. Jeon, *J. Mater. Chem.*, 2012, **22**, 5374.
16 Z. P. Ci, M. D. Que, Y. R. Shi, G. Zhu, Y. H. Wang, *Inorg. Chem.*, 2014, **53**, 2195.
17 L. Juan, D. P. Fu, Z. Rui, H. L. Yan, J. S. Hyo, *J. Mater. Chem.*, 2011, **21**, 16398.
18 H. L. Jee, J. K. Young, *Mater. Sci.Eng. B*, 2008, **146**, 99.
19 O. Emel, K. Semra, *Ceram. Int.*, 2010, **36**, 1033.
20 M. A. Camerucci, G. Urretavizcaya, M. S. Castro, A.L. Cavalieri, *J.Eur.Ceram.Soc.*, 2001, **21**, 2917.
21 K. N. Milan, C. Minati, *J.Eur.Ceram.Soc.*, 2004, **24**, 3499.
22 G. P. Thim, H. F. Brito, S. A. Silva, M. A. Olivelra, M. C. Felin, *J. Solid State Chem.*, 2003, 171, 375.
23 Y. Kamiyanagi, M Kitaura, M. Kaneyoshi, *J. Lumin.*, 2007, **122**, 509.
24 B. Liu, L. J. Kong, C. S. Shi, *J. Lumin.*, 2007, **122**, 121.
25 L. Lin, M. Yin, C. S. Shi, W. P. Zhang, *J. Alloys Compd.*, 2008, **455**, 327.
26 K. N. Shinde, S. J. Dhoble, K. Animesh, J. Lumin., 2011, **13**, 1931.
27 R. Zhang, X. Wang, *J. Alloys Compd.*, 2011, **509**, 1197.
28 B. E. Douglas, S. M. Ho, *Structure and Chemistry of Crystalline Solids, Springer,* 2006, p.260.
29 G. J. Gao, L. Wondraczek, *Opt. Mater. Express*, 2014, **4**, 476.
30 G. J. Gao, S. Reibstein, M. Y. Peng, L. Wondraczek, *J. Mater. Chem.*, 2011, **21**, 3156.
31 R. D. Shannon, *Acta Crystallogr. A*, 1976, **32**, 751.
32 S.V.S. Sai, S. Vepa, M.U. Arun. *J. Am. Ceram. Soc.*, 1993, **76**, 1873.
33 F. H. Tang, J. D. Zhuang, F. Fei and Q. Liu, Chin. *J. Chem .Phys.*, 2012, **25**, 345.
34 J. L. Cai, R Y Li, C. J. Zhao, S. L. Tie, X. Wan, J. Y. Shen, *Opt. Mater.*, 2012, **34**, 1112.
35 I. Omkaram, S. Buddhudu, *Opt Mater.*, 2009, *32*, 8.
36 F. P. Du, Y. Nakai, T. J. Tsuboi, Y. L. Huang, H. J. Seo., *J Mater Chem*, 2011, **21**, 4669.
37 C. H. Huang, T. M. Chen, W. R. Liu, Y. C. Chiu, Y. T. Yeh, S. M. Jang. *ACS Appl Mater Interfaces*, 2010, **2**, 259.
38 G.Blasse, *Philips Res. Rep.*, 1969, **24**, 131-144.
39 X. M. Liu, C. K. Lin, J. Lin, *Appl. Phys. Lett.*, 2007, **90**, 081904.
40 G. J. G, L, Wondraczek, *Opt. Mater. Express*, 2013, **3**, 633.
41 G. J. G, L, Wondraczek, *J. Mater. Chem.*, 2013, **1**, 1952.
42 Y. S. Tang, S. F. Hu, C. C. Lin, N. C. Bagkar, R. S. Liu, *Appl.Phys. Lett.*, 2007, **90**, 151108.
43 V. Bachmann, C. Ronda, O. Oeckler, W. Schnick, A. Meijerink, *Chem. Mater.*, 2009, **21**, 316.
44 H. Luo, J. Liu, X. Zheng, L. Han, K. Ren, X. Yu, *J. Mater. Chem.*, 2012, **22**, 15887.
45 R. J. Xie, N. Hirosaki,T. Suehiro, F. F. Xu, M. Mitomo, *Chem. Mater.*, 2006, **18**, 5578.